Attraction-Repulsion Model-Based Subpixel Mapping of Multi-/Hyperspectral Imagery

Xiaohua Tong, Xue Zhang, Jie Shan, *Member, IEEE*, Huan Xie, and Miaolong Liu

***Abstract*—This paper presents a new subpixel mapping method based on subpixel attraction-repulsion. The proposed method is formulated as an optimization problem with respect to attraction-repulsion among subpixels and is used to reconstruct a finer spatial resolution image from a lower resolution one. A comprehensive experiment is conducted to demonstrate the performance of the proposed method, by comparing it with the other three existing subpixel mapping methods, i.e., linear optimization, pixel swapping and spatial attraction model methods. In the experiment, both a synthetic image with known fractional abundances and an EO-1 Hyperion hyperspectral image of Shanghai were used to evaluate performances of the subpixel mapping methods. The experimental result shows that by using spatial dependence with attraction between the same types of ground objects and repulsion between different types of these objects, the proposed subpixel mapping method achieves a better performance on subpixel mapping than the other three methods.**

***Index Terms*—Attraction-repulsion model, endmember, spectral mixture model, subpixel mapping.**

I. Introduction

With the emergence of more Earth observation satellites, remote sensing imagery has been increasingly used in many applications, including land cover detection, environmental monitoring, and mineral exploration. A common problem associated with the application of satellite images, however, is the frequent occurrence of mixed pixels [1]. Mixed pixels may be attributed to the presence of small subpixel objects, for example, small areas of wetland in a dry land environment, or to the mixed spectral response of edge pixels, such as along the contact line between two spectrally different land cover types [2], [3]. These mixed pixels pose a difficult problem for land cover mapping and greatly restrict image recognition accuracy, as their spectral characteristics are not representative of any single land cover type. Therefore, it is important to enhance image spatial resolution, principally by software methods, while retaining spectral feature information within the constraints of current hardware technology [4].

To identify mixed pixels, many subpixel level classifiers have been proposed using spectral mixture analysis. This analysis assigns a pixel to several land cover types, in proportion to the area of the pixel that each type covers. Many researchers have addressed this spectral mixture problem. Among the most common techniques for subpixel-based soft classification are independent component analysis [5], [6], the conventional spectral angle mapper [7], linear spectral mixture analysis [8]–[18], nonlinear spectral mixture analysis [19], [20], Gaussian mixture discriminated analysis [21], and artificial neural networks [22]–[24].

As a subpixel-based soft classification, spectral unmixing estimates the proportions of land cover types within each pixel. The result is a series of fraction abundance images of each land cover type. Although spectral unmixing can locate all types of land cover in each pixel with varying proportions, it does not indicate how those types are spatially distributed within the pixel. As a result, there will be a loss of spatial information in remote sensing imagery. This loss can severely hamper the accuracy of image processing. It is essential that subpixel mapping determine the most likely locations of the fraction abundance of each land cover type within the pixel [25]. Simplified methods termed "hard classification" [26], [27] may be used to convert the fraction abundance into a traditional land cover image, wherein the pixel would be assigned to a specific land cover type according to the dominance occupancy by fraction abundance. However, this would result in loss of spatial detail in the same way as traditional hard classifiers, which ignore much ground object information in a one-class-per-pixel land cover image [28].

Atkinson [28], [29] introduced the concept of subpixel mapping using the pixel swapping algorithm as an alternative solution to the problem. Taking the fraction abundance image as initial data, subpixel mapping can retrieve an appropriate spatial location for land cover fractions from soft classification [30]. This approach divides pixels into several smaller units and assigns a land cover to units at the subpixel level, and spatial dependence between pixels in the original image is applied to locate a subpixel of a specific land cover. At the same time, the number of subpixels is assigned to the corresponding proportion of endmember fraction in a mixed pixel. The spectral mixture analysis-based subpixel location method can also perform super-resolution mapping of land cover at a spatial resolution finer than the pixel size of the original image.

Manuscript received September 11, 2011; revised February 11, 2012 and June 20, 2012; accepted July 21, 2012. Date of publication November 12, 2012; date of current version April 18, 2013. The work described in this paper was substantially supported by the National Natural Science Foundation of China (Project 41171352), National key Basic Research Program of China (973 Program) (Project 2012CB957701), High-tech Research and Development Program of China (Project 2012AA12130 and 2012AA120905), and Shanghai Outstanding Academic Leaders Program (Project 12XD1404900).

X. Tong, X. Zhang, H. Xie, and M. Liu are with the College of Surveying and Geo-Informatics and Center for Spatial Information Science and Sustainable Development Applications, Tongji University, Shanghai 200092, China (e-mail: xhtong@tongji.edu.cn; ejau@163.com; huanxie@tongji.edu.cn; liuml@tongji.edu.cn).

J. Shan is with the Department of Geomatics Engineering, School of Civil Engineering, Purdue University, West Lafayette, IN 47907-2051 USA (e-mail: jshan@ecn.purdue.edu).

Color versions of one or more of the figures in this paper are available online at http://ieeexplore.ieee.org.

Digital Object Identifier 10.1109/TGRS.2012.2218612

Following Atkinson, many researchers have proposed subpixel mapping methods that improve image resolution, which are reviewed as follows.

1) Spatial dependence-based algorithms. Several researchers obtained subpixel mapping images based on spatial dependence between subpixels and pixels, by creating new rules to assign the subpixel to a specific land cover type at the location, or by improving the Atkinson's pixel swapping algorithm. Based on the assumption of spatial dependence, Verhoeye and de Wulf [25] proposed a subpixel mapping method with linear optimization technique, to assign several fraction values to subpixels and to generate a land cover map at the subpixel level. Verhoeye and de Wulf's approach is also regarded as a geostatistics method. Mertens *et al.* [31] presented a subpixel mapping algorithm based on the spatial attraction model to produce hard classifications at higher resolution. In the algorithm, spatial dependence was assumed to be a neighborhood of pixels attracting subpixels, and the attraction between subpixel or pixel was used to assign subpixel location to maximize the attractive interaction. Makido *et al.* [32] proposed three improved pixel swapping-based methods to achieve the spatial distribution of multiple land cover classes in subpixel images: 1) Sequential categorical swapping, a modification of a binary pixel swapping algorithm, locates each class in turn to maximize internal spatial correlation. 2) Simultaneous categorical swapping, which simultaneously examines all pairs of cell-class combinations within a pixel to determine the most appropriate pairs of subpixels to swap. 3) Simulated annealing to swap cells. Comprehensive experiments showed that the simulated annealing-based pixel swapping approach has greater flexibility than 1) or 2), although its convergence is relatively slow. Makido and Shortridge [33] improved the pixel-swapping optimization algorithm of Atkinson for mapping subpixel land cover images. Two different simulation models were used to develop spatially correlated binary class raster images. These images were then resampled to generate a series of representative medium-resolution class images. The relationship between subpixel image resolution and spatial correlation was analyzed to locate the subpixels. Shen *et al.* [34] proposed a novel pixel-swapping algorithm to reduce computation time and to improve subpixel mapping accuracy. That algorithm has an initialization based on a subpixel/pixel spatial attraction model, and locates the subpixels of multiple land cover types.
2) Fuzzy algorithms. Many efforts have been made to map subpixel images with fuzzy classifiers or fuzzy algorithms integrated with the pixel-swapping method. Foody [35] presented an image sharpening-based fuzzy subpixel soft classifier that acquires the subpixel distribution of land covers. Thornton *et al.* [36] proposed a supervised fuzzy c-means algorithm within the pixel swapping algorithm, to generate subpixel imagery at fine spatial resolution. In this method, mathematical morphology was used to suppress error in the subpixel mapping.
3) Geostatistics approaches. As stated above, Verhoeye and de Wulf [25] proposed a geostatistics approach with linear optimization technique to achieve the subpixel mapping image. Kasetkasem *et al.* [37] used a Markov random field model-based approach to generate super-resolution land cover maps from remote sensing data. They showed significant improvement in the accuracy of land cover maps with finer spatial resolution, compared to that achieved by the linear optimization of Verhoeye and Wulf [25]. Boucher and Kyriakidis [38], [39] proposed a super-resolution land cover mapping based on the geostatistical method of kriging and stochastic simulation indicators. They also used a cokriging indicator to estimate pixel probability at higher spatial resolution, and their method was used for a specific land cover type, based on fraction abundances with lower spatial resolution. Debella-Gilo and Kääb [40] evaluated the performance of two fundamentally different approaches to achieve a subpixel precision of normalized cross-correlation, by measuring surface displacements of mass movements from repeat optical images. They first interpolated image intensities to a desired subpixel resolution, using bicubic interpolation prior to the actual displacement matching. The image pairs were then correlated at the original image resolution, and peaks of the correlation coefficient surface were located at the desired subpixel resolution using three techniques—bicubic interpolation, parabola fitting, and Gaussian fitting.
4) Image fusion methods. Image fusion of spatial and spectral information is also an effective approach to map subpixel images. Gross and Schott [41], [42] proposed an image sharpening method based on an accurate image fusion algorithm that integrates spectral and spatial information of an image, thereby attaining higher resolution images from lower resolution hyperspectral images.
5) Intelligent algorithms. There are also many artificial intelligence methods to obtain subpixel images. Tatem and Nguyen [43]–[47] improved Hopfield artificial neural networks to acquire subpixel location information. Mertens *et al.* [48] presented a genetic algorithm, combined with the assumption of spatial dependence, to assign a location to every subpixel. The algorithm was tested on synthetic and degraded real imagery, obtaining greater accuracy than with the conventional hard classifications. The method of Mertens *et al.* [30] uses wavelets and artificial neural networks. Their wavelet multi-resolution analysis facilitates the link between different resolution levels, and a higher resolution image is constructed after estimation of detailed wavelet coefficients with neural networks.
6) Sensor response model-based approaches. As an alternative to image-based methods, some approaches are based on geometrical models of sensors to map subpixel images. Ruiz and Lopez [49] used the point spread function [50] of the SPOT sensor to obtain the spatial location of urban land cover subpixels, based on de-convolution filtering. Kaiser and Schneider [51] performed spatial subpixel analysis to enhance images of fine-structured

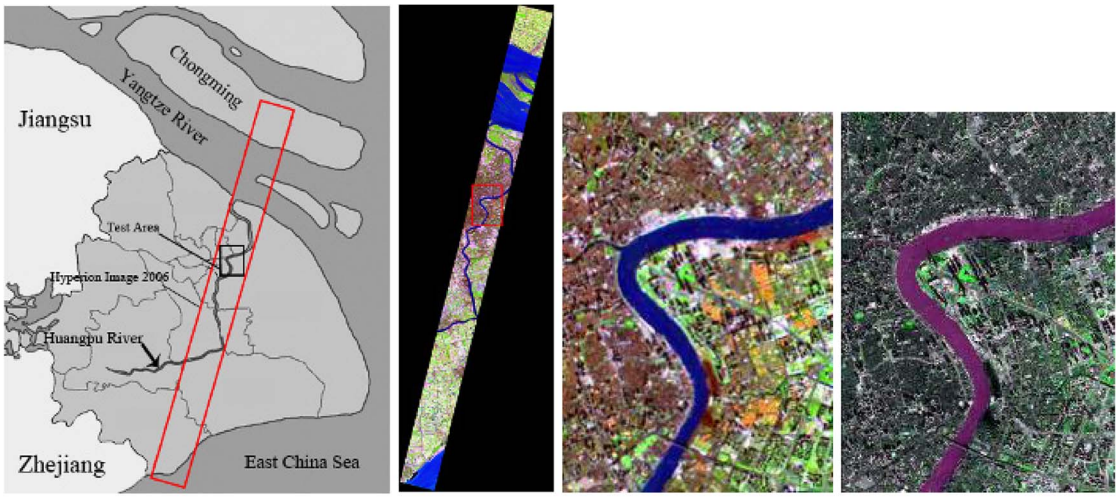

Fig. 1. Study area and experimental imagesa. (a) Study area. (b) Hyperion image from 2006 (a false color image composed of R:203, G:53, B:23). (c) Partial Hyperion image taken from (b). (d) Partial QuickBird image corresponding to (c).

landscapes, based on geometric description of object boundaries that intersect pixels and thus lead to mixed pixels. They found that the spectrum value of any mixed pixel depends on sensor spatial response, as well as corresponding geometric characteristics of land cover distribution.

With regard to the aforementioned approaches, there are some shortcomings for existing subpixel mapping methods, as follows. 1) Spatial dependence simply accounted for the attractive relationship between the same ground objects, which is regarded as subpixel attractiveness in [28], [29], and [34] and as subpixel/pixel attraction by Mertens *et al.* [31]. However, the repulsion between different ground objects should also be considered as a spatial dependence relationship. 2) Sensitivity to the scale factor of subpixel mapping. When the scale factor of subpixel mapping increases, the spatial location of subpixels tends to be incorrect, particularly at a larger scale factor, resulting in unsustainable mapping accuracy. 3) Sensitivity to initialization of the location of subpixels. Because of the sensitivity to the random initialization procedure that begins the location of subpixels, stability and accuracy of the subpixel mapping degrades.

Therefore, a new subpixel mapping method based on subpixel attraction-repulsion is presented here. In contrast to the traditional subpixel mapping methods, the proposed method makes use of spatial dependence with not only attraction between the same kinds of ground objects, but also repulsion between different kinds of these objects. In the study, both a synthetic image with known fractional abundances and an EO-1 Hyperion hyperspectral image of Shanghai are used to evaluate performance of the proposed method, through comparison with the other subpixel mapping methods. Like these other methods, the proposed one is capable of processing multiple fractions of land cover types for representing ground truth in detail. Moreover, the proposed method can achieve a subpixel image with robust accuracy at multiple scale factors, particularly in the case of a larger scale factor.

II. Study Area and Data Used

The city of Shanghai, on the eastern Yangtze River estuary, was chosen as the study area [Fig. 1(a)]. This is a typical urban area with a mixture of land cover types, i.e., water, vegetation, impervious surface, soil, and shade. Vegetation type can be subdivided into high moisture and low moisture, and impervious surface type into high albedo impervious and low albedo impervious.

In the study, one strip of a Hyperion hyperspectral image [Fig. 1(b)] from November 8, 2006 was used. Its size is 1091 $\times$ 3461 pixels, with spatial resolution of 30 m by 30 m. A total of 155 "stable" bands out of the 242 bands in the image were used for subpixel mapping. The selected bands avoided most residual atmospheric noise effects [52]. The test data presented in Fig. 1(c) are a subset of the entire image strip in Fig. 1(b), covering an area of 192 $\times$ 268 pixels. In addition, one QuickBird multi-spectral image [Fig. 1(d)] with spatial resolution 2.4 m, obtained in September 2006, was used as a reference map and geo-registered to the Hyperion image. All experimental data are labeled in Fig. 1(a).

III. Methodology

Fig. 2 shows the entire methodology for the study. There are three main parts, as follows: 1) Subpixel mapping based on the subpixel attraction-repulsion model; 2) accuracy assessment of subpixel mapping based on the schematic diagram explanation, visual comparison and quantitative assessment; and 3) analysis of impact of the spectral mixture model on the accuracy of subpixel mapping.

Assuming that the number of land cover types is C, the idea of the proposed subpixel mapping method and its operational rules are addressed as follows.

A. Achieving Fraction Abundance of Land Cover Type

The source of fraction abundance images used for subpixel mapping is obtained from the result of spectral mixture analysis of land covers in Tong *et al.* [53].

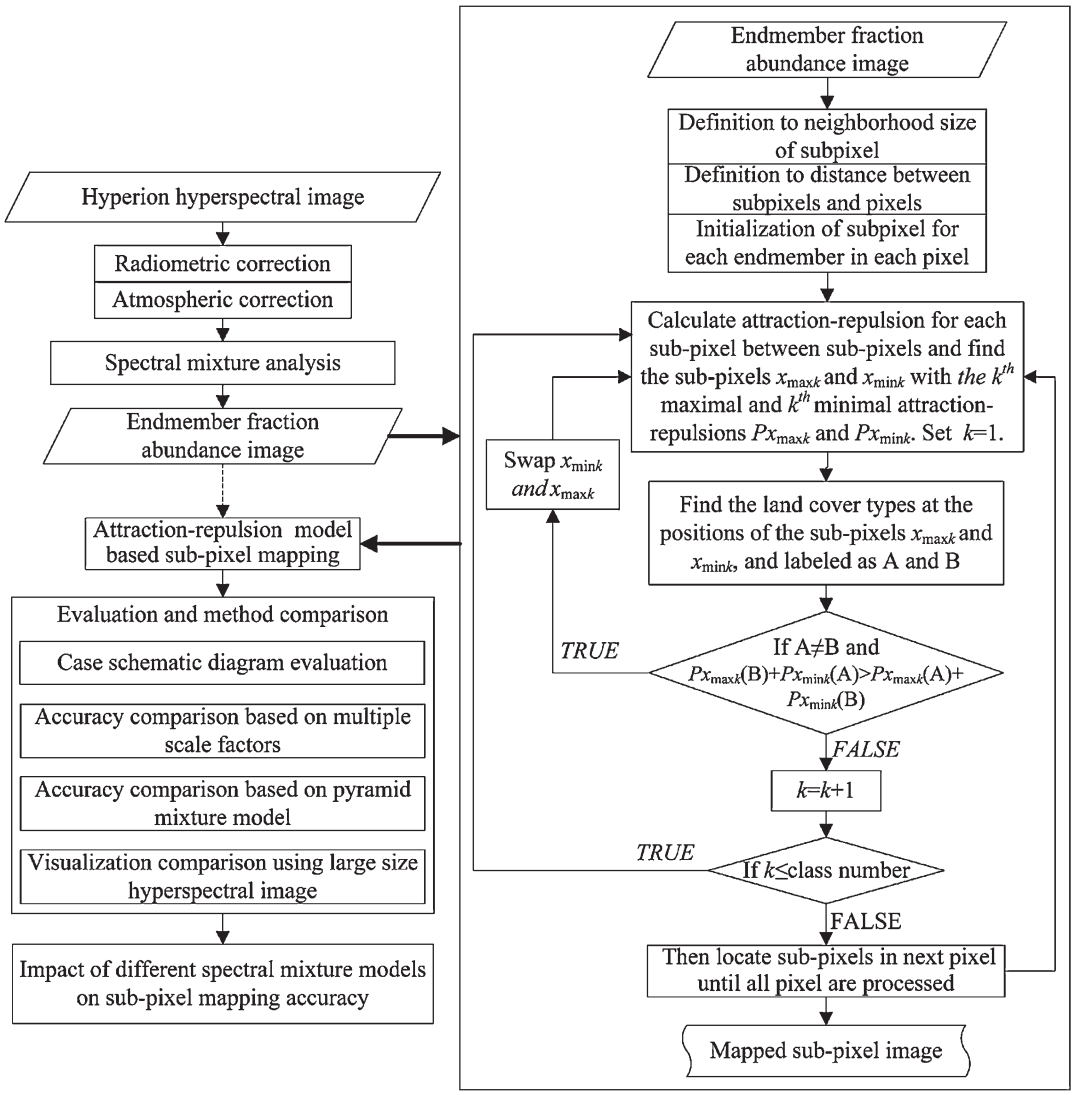

Fig. 2. Methodology of the study.

B. Initialization of Subpixels

The number of subpixels for each land cover type is calculated based on the obtained fraction abundance in each pixel, and it remains constant throughout the subpixel location and adjustment process. The scale factor $\varsigma = n$ (i.e., each pixel is divided into $n \times n = n^2$ subpixels) also remains constant during algorithm processing. Therefore, the spatial resolution of the generated subpixel image with specific scale factor can be computed as S/ς, where S is spatial resolution of the original image, from which the fraction abundance is achieved. Initially, subpixel positions are located either in sequence [Fig. 3(b)(1)], or randomly [Fig. 3(b)(2)].

In Fig. 3, the quality of a single subpixel is assumed to be 1, and the total subpixel quality of each land cover type in a pixel is equivalent to the number of subpixels for that land cover type in the pixel.

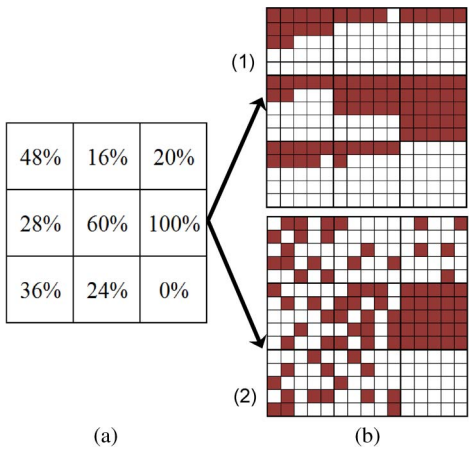

Fig. 3. Initialization of subpixel mapping. (a) Fraction abundance, and (b) initial location of subpixels (in case with scale factor $\varsigma = 5$); (b)(1) denotes initial location in sequence, and (b)(2) initial random location.

C. Calculation of Attraction-Repulsion Between Two Subpixels

Based on the computed number of subpixels and their initialization, attraction-repulsion between two subpixels, or that between a subpixel and pixel, is calculated according the pixel neighborhood. A neighborhood of 3 × 3 pixels is used for the attraction-repulsion computation, and subpixels

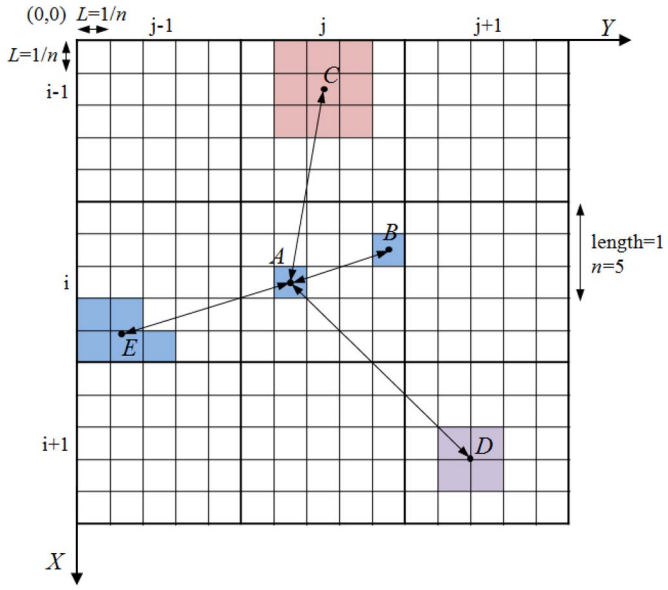

Fig. 4. Definition of distance calculation between subpixels in a pixel, and between pixels and subpixels ($\varsigma = 5$). Adapted from Mertens *et al.* [31].

of other pixels outside this neighborhood are not considered in this computation. The attraction-repulsion calculation between subpixels (pixels) follows the rule that the same materials attract each other, while different ones repel. Therefore, the attraction-repulsion between two subpixels is expressed by

$$p_{12} = k \cdot \frac{m_1 m_2}{r_{12}^2} \tag{1}$$

where p_{12} is the attraction or repulsion, m_1 and m_2 are qualities of two subpixels (pixels), respectively, r_{12} is the distance between two subpixels within the same pixel, or the distance between a subpixel in one pixel and a subpixel(s) in another pixel, and k is the attraction-repulsion factor.

1) Distance Calculation Between Two Subpixels: The distance calculation is critical in the attraction-repulsion model. For a given scale factor ς, there are generally two cases for calculating distance between two subpixels. Fig. 4 shows the definition of distances when $\varsigma = 5$. The first case is when the two subpixels are within the same pixel; their distance is defined as that between their center points, for example the distance between A and B in Fig. 4. The second case is that when the subpixels are within two different pixels; their distance is defined as that between the center point of the current subpixel within one pixel and the average position of the subpixels within the other pixel, for example the distances between A and C, D, E in Fig. 4.

In the figure, the unit length of a subpixel is defined as $L = 1/n$ for the scale factor $\varsigma = n(n = 5)$. Therefore, points A and B are center points of the two subpixels in the current pixel (i, j), and points C, D, and E are average positions of the subpixels in pixels $(i-1, j)$, $(i+1, j+1)$ and $(i, j-1)$, respectively. Assuming in Fig. 4 that each pixel is divided into $n \times n = n^2$ subpixels, the area of each subpixel is $1/n^2$, which corresponds to the fraction abundance for a specific land cover type. The average position of subpixels within the same pixel is calculated by

$$\begin{cases} \bar{x} = \frac{1}{m} \sum_{i=1}^{m} x_i \\ \bar{y} = \frac{1}{m} \sum_{i=1}^{m} y_i \end{cases} \tag{2}$$

where $(\overline{x}, \overline{y})$ are coordinates of the average position, (x_i, y_i) are coordinates of subpixels belonging to the same land cover type within a pixel, and m is the number of subpixels. Thus, coordinates of points A, B, C, D, and E in Fig. 4 are represented by

$$\begin{cases} A : (i - 1 + 5/2n, j - 1 + 3/2n) \\ B : (i - 1 + 3/2n, j - 1 + 9/2n) \\ C : (i - 2 + 3/2n, j - 1 + 5/2n) \\ D : (i + 3/n, j + 2/n) \\ E : (i - 1 + 41/10n, j - 1 + 13/10n). \end{cases} \tag{3}$$

Thus, the distances between point A and points B, C, D, and $E$are calculated by

$$d(s,t)^2 = (x_s - x_t)^2 + (y_s - y_t)^2 \tag{4}$$

where (x_s, y_s) are the coordinates of point A, and (x_t, y_t) are the coordinates of points B, C, D, or E, as represented in (3).

2) Calculation of Attraction-Repulsion Values: In the process of subpixel mapping based on the attraction-repulsion model, attraction-repulsion values are iteratively calculated to adjust the location of each subpixel. When calculating the attraction-repulsion value p between two subpixels, k in (1) is set to 1 for subpixels of the same land cover types, and -1 for subpixels of different land cover types.

D. Location for Subpixels

Based on the aforementioned rule, subpixels are iteratively adjusted at different positions within a pixel to make the total attraction-repulsion value (P) maximal

$$\max P = \sum_{k=1}^{N \times M} P_k \tag{5}$$

$$P_k = \sum_{t \neq k}^{N \times M} p_{kt} \tag{6}$$

where N is the number of image pixels in a pixel neighborhood, M is the number of subpixels in each pixel, P_k is the resultant attraction-repulsion value of the kth subpixel, and p_{kt} is the attraction-repulsion value between subpixels k and t, as computed by (1). If the total attraction-repulsion values for all pixel neighborhoods are maximized, then the final subpixel image would be the objective image result with improved spatial resolution. Moreover, in the process of subpixel mapping based on the attraction-repulsion model, subpixel location adjustment includes a series of iterations for subpixel swapping. Fig. 5 shows a schematic diagram of the process of subpixel mapping, for four land cover fractions.

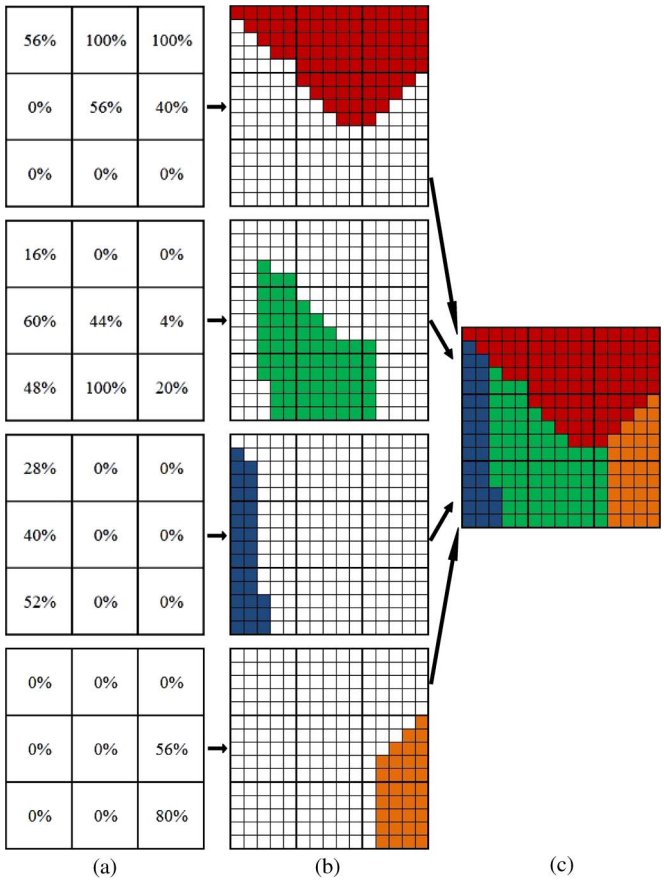

Fig. 5. Process of subpixel mapping in a 3 × 3 pixel scene, adapted from Atkinson [28]. (a) Fraction abundance of four land cover types, (b) location of subpixels for each fraction in subpixel mapping, and (c) location of subpixels in pixel neighborhood, through subpixel mapping.

During the process of swapping subpixels in the current pixel, assume that $x_{i\max}$ is the position of the subpixel corresponding to the maximum resultant attraction-repulsion value $P_{\max}(i)$ for the ith land cover type, and $x_{j\min}$ is the position of the subpixel corresponding to the minimum resultant attraction-repulsion value $P_{\min}(j)$ for the jth land cover type. Thus, based on (1), $x_{i\max}$ and $x_{j\min}$ are calculated by

$$x_{i\max}=\{x\in x_{ik}|P_{\max}(i)=\max\left(P_k(i)\right),k=1,2,\ldots,S_i\} \quad (7)$$

$$x_{j\min}=\{x\in x_{jk}|P_{\min}(j)=\min\left(P_k(j)\right),k=1,2,\ldots,S_j\} \quad (8)$$

where $P_k(i)$ and $P_k(j)$ are resultant attraction-repulsion values for the kth subpixel of the ith and jth land cover types in the current pixel, respectively; and S_i and S_j are the numbers of subpixels of the ith and jth land cover types.

Accordingly, positions of the two subpixels corresponding to the maximum and minimum resultant attraction-repulsion values ($x_{\max}$ and $x_{\min}$) of all subpixels, for all land cover types in the current pixel, are calculated by

$$x_{\max}=\{x\in x_{i\max}|P_{\max}=\max\left(P_{\max}(i)\right),i=1,2,\ldots,C\} \quad (9)$$

$$x_{\min}=\{x\in x_{j\min}|P_{\min}=\min\left(P_{\min}(j)\right),j=1,2,\ldots,C\} \quad (10)$$

where C is the number of land cover types.

Assuming that land cover types at positions $x_{\max}$ and $x_{\min}$ are a and b; thus, the two subpixels at $x_{\max}$ and $x_{\min}$ are swapped if $P_{x_{\max}}(b)+P_{x_{\min}}(a)>P_{x_{\max}}(a)+P_{x_{\min}}(b)$ (where $a\neq b$). Otherwise, the subpixels are not swapped. Positions of the two subpixels with the second maximum and minimum resultant attraction-repulsion values in the current pixel are subsequently labeled and attained, for executing the next adjustment process. The adjustment process is repeated until a total of C adjustments are conducted for the current pixel (C is the number of land cover types); the process then transfers to the next pixel in the neighborhood. The termination rule in a neighborhood can be customized by setting the maximum number of iterations for each neighborhood, or specified based on convergence, for which the optimum total attraction-repulsion value satisfying (5) is pre-defined. Therefore, when the total attraction-repulsion values of all pixel neighborhoods are maximal, as presented in (5), the optimal subpixel image is obtained, and each subpixel is located with the best position.

E. Evaluation and Experiments

To evaluate performance of the proposed subpixel mapping method, we compare the proposed method with the three existing ones. Those three are as follows. 1) The linear optimization subpixel mapping method of Verhoeye and de Wulf [25]. 2) Atkinson's pixel-swapping subpixel mapping algorithm [28], [29], [34]. 3) The spatial attraction model-based subpixel mapping method of Mertens *et al.* [31]. Fig. 1(c) shows a subset of a Hyperion hyperspectral image used in the comparison. In addition, a synthetic image was used to evaluate performance of the four subpixel mapping methods. Moreover, three approaches were used to assess the error of these four methods—the schematic diagram, visualization assessment, and quantitative analysis. Error assessment of the four methods based on the Hyperion hyperspectral image was done in two ways. The first is use of a QuickBird multi-spectral image as reference data, and the second is based on the pyramid mixture model.

Errors of the four subpixel mapping methods at multiple scale factors were evaluated with the reference data set, using a stratified, systematic random sampling method [54]. When a subpixel mapping is conducted at a scale factor, e.g., $\varsigma=2$, spatial resolution of the mapped image would be 15 m. A total of 50 sample units were collected from the mapped image for error assessment, and each sample unit was 3 × 3 pixels. The QuickBird image with spatial resolution 2.4 m was resampled to 5 m resolution, and a corresponding sample unit of 9 × 9 pixels was obtained from the reference image covering the same area as the mapped image. For each sample unit, a pixel at a given position in the mapped image is scaled to determine ground truth land cover type, by comparing pixels at the same position in the reference image. The reference image was generated from a hard classification of the resampled QuickBird image, and the fraction abundance of each land cover type in the pixel was calculated in the sample unit. These fraction abundance images were used as input for subpixel mapping, and the hard-classified image from the QuickBird image used as reference data for assessing the error of subpixel mapping. Therefore, with the given spatial samples and located subpixels

in the mapped images, overall accuracy (A) of the subpixel mapping method and its root mean square (RMS) errors (ε) are calculated by

$$A = \sum_{k=1}^{C} A_k / C \tag{11}$$

$$\varepsilon = \sum_{k=1}^{\mathrm{C}} (\varepsilon_k - \overline{\varepsilon}) / C \tag{12}$$

where C is the number of land cover types, A_k and $\varepsilon_k = 1 - A_k$ are percentages of correct location and wrong location of subpixels for the kth land cover type, and $\overline{\varepsilon} = \sum_{k=1}^{C} \varepsilon_k / C$ is the average percentage of wrong location of subpixels for all land cover types. Similarly, for any scale factor (from $\varsigma = 2$ to $\varsigma = 8$), error assessment of subpixel mapping is conducted by comparing the mapped image with the reference one.

The overall accuracy in (11) indicates the total precision of subpixel location. The RMS error in (12) measures the difference between location values of subpixels based on the four subpixel mapping methods and actual values observed from spatial sampling units in the reference image. It is clear that the percentage of correct location in subpixel mapping increases overall accuracy and simultaneously decreases RMS error.

IV. Results and Discussion

A. Error Assessment of Subpixel Mapping Based on Schematic Diagram

In this section, two cases in terms of scale factor are illustrated with schematic diagrams, to assess performance of the proposed subpixel mapping method by comparison with the other three methods. The first case is for scale factor $\varsigma = 3$ (Case I), the second for $\varsigma = 5$ (Case II). Fig. 6 shows a comparison of schematic diagrams between the proposed attraction-repulsion model and the attraction model [31], for the two cases.

In Fig. 6, two 3×3 pixel neighborhoods were used for both cases. Subpixels in the center pixel of both neighborhoods were located through swapping position or assigning with a land cover type. In both cases, because no unique accurate solutions could be achieved using the linear optimization subpixel mapping method, we only compared the pixel swapping, spatial attraction model and our proposed attraction-repulsion model-based methods. Determination metrics of final neighborhood status shown in Fig. 6 were calculated using the three subpixel mapping methods. Table I shows these metrics for the three methods, in the two cases. In the table, $\boldsymbol{P}_{\mathrm{attactiveness}}$ is the determination metric of the pixel swapping method, $\boldsymbol{P}_{\mathrm{attaction}}$ is that of the spatial attraction model method, and $\boldsymbol{P}_{\mathrm{attaction-repulsion}}$ is that of our method.

Fig. 6(a)(1) and (b)(1) show results based on the pixel swapping and spatial attraction model methods, which only account for spatial dependence of the attractive relationship. Fig. 6(a)(2) and (b)(2) show results based on the proposed method that considers spatial dependence of both attractive and

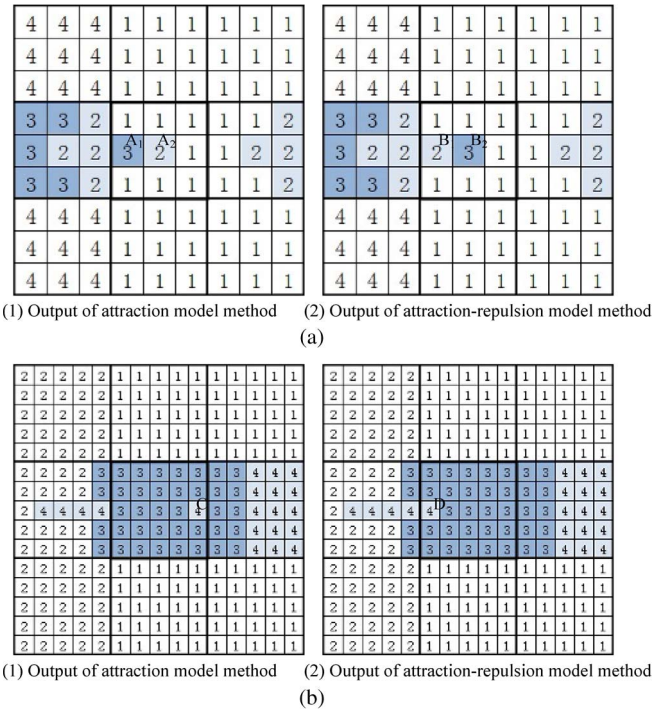

Fig. 6. Comparison of schematic diagrams between proposed attraction-repulsion model and attraction model, in two scale factor cases ($\varsigma = 3$ and $\varsigma = 5$). (a) Case I: Comparison between attraction model and attraction-repulsion model as $\varsigma = 3$; (b) Case II: Comparison between attraction model and attraction-repulsion model as $\varsigma = 5$.

TABLE I
Determination Metrics of Three Subpixel Mapping Methods in the Two Cases

	Case I		Case II	
	Fig.6(a)-(1)	Fig.6(a)-(2)	Fig.6(b)-(1)	Fig.6(b)-(2)
$\boldsymbol{P}_{\mathrm{attactiveness}}$ by pixel swapping method	25.9366	25.7932	84.5850	83.4908
$\boldsymbol{P}_{\mathrm{attaction}}$ by spatial attraction model method	3.3179	3.3144	10.1515	10.1036
$\boldsymbol{P}_{\mathrm{attaction-repulsion}}$ by our proposed method	14.2272	15.0327	2348.6815	2366.0534

repulsive relationships. In Case I, as shown in Fig. 6(a)(1), the subpixel A_1 labeled "3" is located closer to those five subpixels labeled "3" in a left pixel, aiming to achieve a greater attraction between the current pixel and its neighborhood pixels based on the attraction model method. However, repulsion of subpixel A_1 labeled "3" from the four subpixels labeled "2" in the left pixel is neglected, causing isolation of the subpixel A_2 labeled "2" from the four subpixels labeled "2" in the left pixel. Using the proposed method, as shown in Fig. 6(a)(2), the subpixel A_2 labeled "2" is grouped with the four subpixels labeled "2" in the left pixel. In Case II, as shown in Fig. 6(b)(1), the subpixel C labeled "4" is located much closer to the subpixels labeled "4" in the right pixel, based on the attraction model method. However, this result isolates subpixel C from the four subpixels labeled "4" in the left pixel and produces a hole

within the subpixels labeled "3" to maximize attraction between the current pixel and its neighborhood pixels. Therefore, as shown in Fig. 6(b)(2), using the proposed method, subpixel D labeled "4" is grouped with the homogeneous four subpixels labeled "4" in the left pixel.

From the results in Fig. 6 and Table I, we see that the result in Fig. 6(a)(2) and (b)(2) describes stronger spatial dependence than that in Fig. 6(a)(1) and (b)(1). The reason for this trend is that the proposed subpixel mapping method groups subpixels of the same land cover type together as much as possible. Therefore, with introduction of attraction and repulsion among subpixels, the proposed method yields the results in Fig. 6(a)(2) and (b)(2) of gathering subpixels. Both the pixel swapping and spatial attraction model methods achieve the results in Fig. 6(a)(1) and (b)(1) of isolating subpixels from the sets of the same kind, toward maximizing the attraction correlation. Consequently, the proposed method is better than both pixel swapping and spatial attraction model methods, in terms of retrieving the spatial dependence of ground truth in such circumstances.

B. Error Assessment of Subpixel Mapping Using Synthetic Data

In this section, performance of the proposed method is demonstrated through comparison with the other three based on a synthetic image. In this image, all fractional abundances are known in advance. The synthetic data was first achieved from hard classification of an artificial image, and it was degraded to one with lower spatial resolution. Area proportions of each land cover type in a pixel were then calculated, and the pixel size adjusted for a specific resolution. The proportions were treated as fraction abundance values, resulting from a soft classification of the synthetic image with lower spatial resolution. These fraction abundance images were finally used as inputs to the subpixel mapping methods, for generating subpixel mapping images. In addition, the original artificial image was used as reference data for evaluating performance of the four subpixel mapping methods. Fig. 7 shows the result of subpixel mapping images generated by the four methods, based on synthetic data with scale factor $\varsigma = 4$. Table II shows overall accuracy and RMS error of the subpixel mapping using the four methods, based on synthetic data at different scale factors ($\varsigma = 2, 3, 4, 5, 6, 7,$ and 8).

From the results in Fig. 7 and Table II, we see that: 1) The spatial attraction model method achieves a better subpixel mapping image than the linear optimization method, in terms of overall accuracy and RMS error. However, the generated images based on both methods are somewhat different from the reference image. 2) The result of subpixel mapping using the proposed method is the best in terms of overall accuracy and RMS error, compared to the other three methods. The subpixel mapping image based on the proposed method is closest to the reference synthetic data. 3) The pixel swapping method achieves the subpixel mapping image closest to the reference data. However, because of some incorrect subpixel locations, both overall accuracy and RMS error are lower than those of our proposed method.

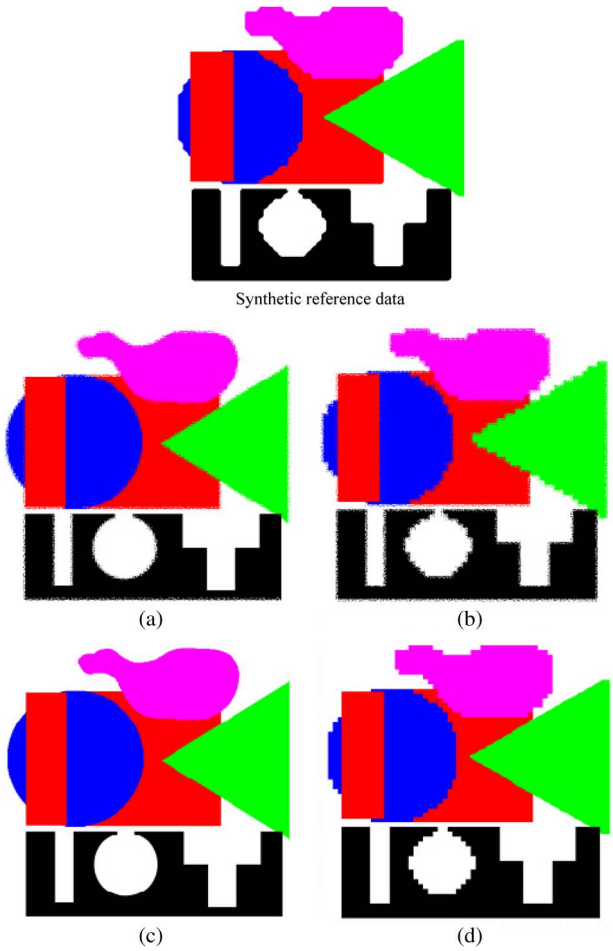

Fig. 7. Mapped subpixel images resulting from the four methods and synthetic data ($\varsigma = 4$). (a) Linear optimization method, (b) pixel swapping method, (c) spatial attraction model method, and (d) our proposed method.

C. Error Assessment of Subpixel Mapping Using Hyperion Hyperspectral Image

Varying scale factors cause different rounding errors, which in turn affect the accuracy of subpixel mapping. In this section, an experiment with different scale factor scenarios was conducted, to analyze scale factor impact on the error of subpixel mapping. Rounding error was produced in this mapping by conversion of the number of subpixels from the floating proportion values in the fraction image. Similar to the evaluation process of subpixel mapping with synthetic data, the reference image was attained from hard classification of the QuickBird image, as shown in Fig. 1(d). Using the reference image, we compared errors of subpixel mapping at different scale factors, i.e., $\varsigma = 2, 3, 4, 5, 6, 7,$ and 8. The 10-EM model was adopted for subpixel mapping, which refers to the spectral mixture model with ten endmember fractions corresponding to ten land cover types. These are: High moisture vegetation, medium moisture vegetation, low moisture vegetation, water, shade, high albedo impervious surface, medium albedo impervious surface, low albedo impervious surface, dry soil, and wet soil. Subpixel images were generated from the original image shown in Fig. 1(c) using the aforementioned four subpixel mapping methods based on the fraction abundance images. Among

TABLE II
OVERALL ACCURACY AND RMS ERROR OF SUBPIXEL MAPPING USING THE FOUR METHODS BASED ON SYNTHETIC DATA

		Scale factor						
		ς=2	ς=3	ς=4	ς=5	ς=6	ς=7	ς=8
Linear optimization	A	65.08%	63.38%	59.63%	53.04%	47.36%	37.71%	27.94%
	ε	0.1219	0.1341	0.1630	0.2205	0.2771	0.3880	0.5193
Pixel swapping	A	77.12%	75.76%	73.60%	69.51%	65.31%	58.15%	48.04%
	ε	0.0523	0.0588	0.0697	0.0930	0.1204	0.1751	0.2699
Spatial attraction model	A	84.28%	83.03%	81.21%	78.94%	73.14%	68.49%	61.56%
	ε	0.0247	0.0288	0.0353	0.0444	0.0721	0.0993	0.1478
Our proposed method	A	92.34%	91.43%	88.71%	87.12%	82.91%	79.62%	77.12%
	ε	0.0059	0.0073	0.0128	0.0166	0.0292	0.0415	0.0523

Notes: For convenience, overall accuracy is denoted by A, RMS error is denoted by ε.

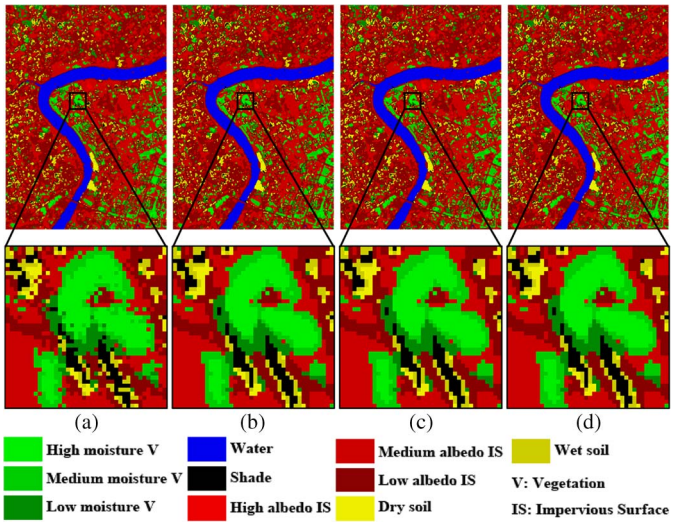

Fig. 8. Mapped subpixel images using the four methods ($\varsigma = 2$). (a) Linear optimization method, (b) pixel swapping method, (c) spatial attraction model method, and (d) our proposed method.

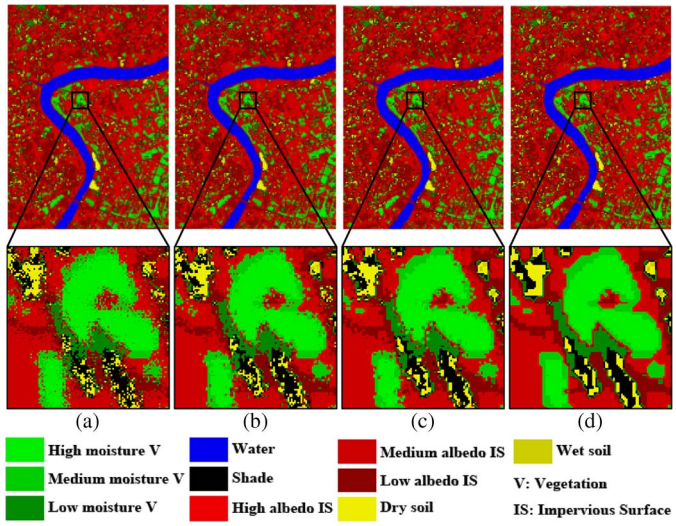

Fig. 9. Mapped subpixel images using the four methods ($\varsigma = 5$). (a) Linear optimization method, (b) pixel swapping method, (c) spatial attraction model method, and (d) our proposed method.

these, three representative mapped subpixel images, with scale factor $\varsigma = 2$, 5 and 8, are presented in Figs. 8–10, respectively.

Visualization quality was compared between the generated images, via the number of isolated pixels and degree of error measure [29], [34]. From the results in Figs. 8–10, we see that: 1) For all four subpixel mapping methods, the larger the scale factor, the poorer the quality of the mapped subpixel image. 2) When $\varsigma = 2$, the subpixel image mapped by the linear optimization method shows the worst clarity of features. The subpixel image mapped by the proposed method shows no significant difference with those mapped by both the pixel swapping and spatial attraction model methods. 3) When $\varsigma = 5$, both linear optimization and pixel swapping subpixel mapping methods produce mapped images with somewhat ambiguous features, although the latter is better than the former. The subpixel image mapped by the spatial attraction model method is similar to that mapped by the proposed method. However, there is some scattering of subpixels in the former image. 4) When $\varsigma = 8$, subpixels in the images mapped by the linear optimization, pixel swapping, and spatial attraction model methods are distributed with great disorder, particularly those generated by the pixel swapping method. However, the image mapped by the proposed method shows much greater clarity of features.

Error of the four subpixel mapping methods at different scale factors was quantitatively evaluated, with the result shown in Table III. Based on this result, Fig. 11 shows curves of overall accuracy for subpixel mapping based on the four methods, at different scale factors.

From the results in Fig. 11 and Table III, it is observed that: 1) When $\varsigma = 2$, the linear optimization method gives the worst subpixel mapping of the four methods, in terms of overall accuracy and RMS error. Both pixel swapping and spatial attraction model methods show better performance than the linear optimization method, in the case of $\varsigma = 2$. However, the proposed method yields the best subpixel mapping result. When the scale factor increases from $\varsigma = 2$ to $\varsigma = 5$, overall accuracy of the mapping declines smoothly for all methods. 2) When $\varsigma = 5$, the linear optimization method shows the worst mapping performance. The proposed method attains the best mapping result, although the spatial attraction model outperforms both the pixel swapping and linear optimization methods. When the scale factor increases from $\varsigma = 5$ to $\varsigma = 8$,

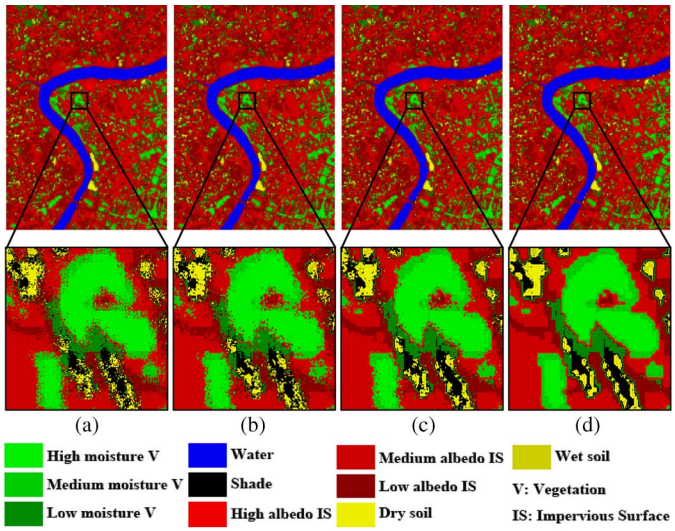

Fig. 10. Mapped subpixel images using the four methods ($\varsigma = 8$). (a) Linear optimization method, (b) pixel swapping method, (c) spatial attraction model method, and (d) our proposed method.

TABLE III
RESULTS OF OVERALL ACCURACY AND RMS ERROR OF SUBPIXEL MAPPING, BASED ON THE FOUR METHODS AT DIFFERENT SCALE FACTORS

		Scale factor						
		ς=2	ς=3	ς=4	ς=5	ς=6	ς=7	ς=8
Linear optimization	A	57.3%	55.8%	52.5%	46.7%	41.7%	33.2%	24.6%
	ε	0.1823	0.1954	0.2256	0.2841	0.3399	0.4462	0.5685
Pixel swapping	A	67.9%	66.7%	64.8%	61.2%	57.5%	51.2%	42.3%
	ε	0.1030	0.1109	0.1239	0.1505	0.1806	0.2381	0.3329
Spatial attraction model	A	74.2%	73.1%	71.5%	69.5%	64.4%	60.3%	54.2%
	ε	0.0666	0.0724	0.0812	0.0930	0.1267	0.1576	0.2098
Our proposed method	A	81.3%	80.5%	78.1%	76.7%	73.0%	70.1%	67.9%
	ε	0.0350	0.0380	0.0480	0.0543	0.0729	0.0894	0.1030

Notes: For convenience, overall accuracy is denoted by A, RMS error is denoted by ε.

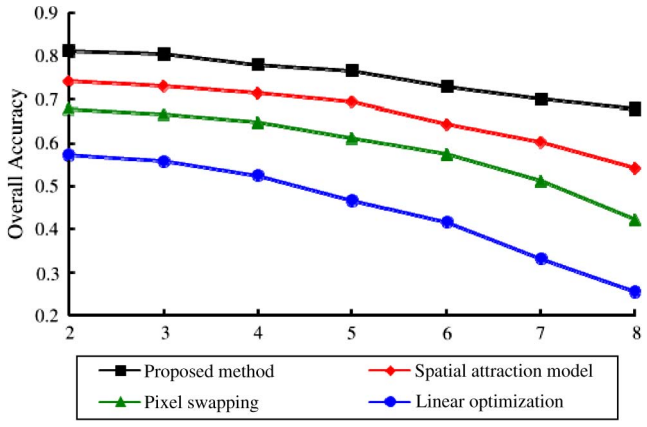

Fig. 11. Curves of overall accuracy for subpixel mapping, based on the four methods at different scale factors.

overall mapping accuracy using the proposed method declines smoothly, whereas this accuracy declines much faster with the other three methods, particularly with linear optimization. 3) When $\varsigma = 8$, the linear optimization, pixel swapping and spatial attraction model methods perform subpixel mapping with decreased overall accuracy. The linear optimization method is particularly poor, with overall accuracy 24.6% and RMS error 0.5685. However, the proposed method still gives the best result in terms of overall accuracy and RMS error.

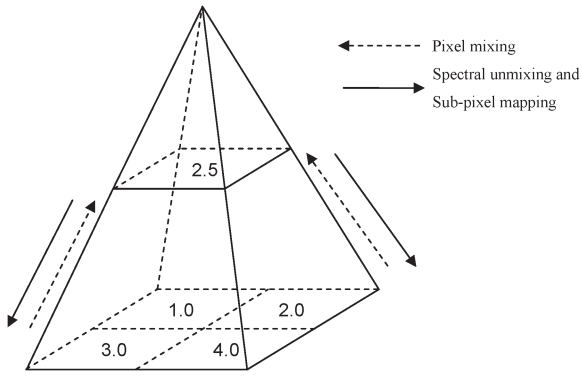

Fig. 12. Pyramid mixture model.

Therefore, both visual assessment of image quality and quantitative comparison of subpixel mapping accuracy reveal that: 1) For all four subpixel mapping methods, the larger the scale factor, the lower the accuracy of the mapping result. 2) The proposed method yields much better results than the other three methods for all scale factors, particularly the larger one.

Error assessment using the reference image can evaluate the performance of all subpixel mapping approaches. However, the error assessment with reference data (QuickBird multi-spectral image), which is dependent on reference image precision, must deal with geometric correction and geo-registration, as well as with dissimilarity between the reference image and reality. This dissimilarity can be caused by various factors, such as the weather at image acquisition time. In the following section, error assessment based on the pyramid mixture model is proposed for evaluating performance of the subpixel mapping approaches.

D. Error Assessment of Subpixel Mapping Based on Pyramid Mixture Model

From the schematic diagram of the pyramid mixture model (Fig. 12), the original experimental image shown in Fig. 1(c) was first produced, with pixel mixing toward a lower resolution image along the direction of the dashed line in the figure. The pixel mixing procedure involved taking any four adjacent pixels of 2×2 window size in the original image to derive a new mixed pixel, for each band of the image. The derived image has half the width and height of the original, and the mixed pixel value in the derived image is the mean spectral value of the four adjacent pixels in the original. Afterwards, the image was conducted spectral unmixing along the direction of the solid line shown in Fig. 12. The spectral unmixing method [53] was used to obtain fraction abundance images based on the 7-EM model, in which the seven fraction abundances are high moisture vegetation, low moisture vegetation, water, shade, high albedo impervious surface, low albedo impervious surface, and soil. Subsequently, the fraction abundance image was used for subpixel mapping at scale factor $\varsigma = 2$, based on the proposed and other three methods. This generated subpixel images of the same size as the original. The pyramid mixing and unmixing

Fig. 13. Pyramid mixture model-derived mixed image, with spatial resolution 60 m × 60 m.

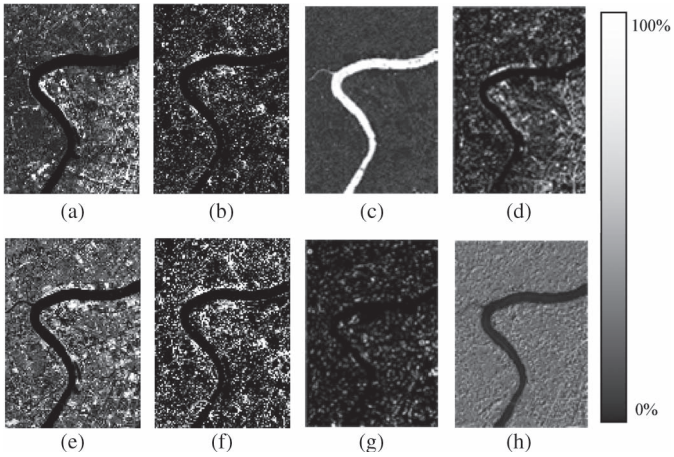

Fig. 14. Fraction abundance images and error image based on mixed image derived from pyramid mixture model. (a) High moisture vegetation, (b) low moisture vegetation, (c) water, (d) shade, (e) high albedo impervious surface, (f) low albedo impervious surface, (g) soil, and (h) error image.

model was used to assess error of the subpixel mapping, by comparing the mapped subpixel image with the original. Fig. 13 shows the mixed image of spatial resolution 60 m × 60 m, as derived from the original experimental image [Fig. 1(c)]. Fig. 14 shows seven fraction abundance images based on the mixed image derived from the pyramid mixture model.

With these fraction abundance images, error for each individual land cover type, overall accuracy of spectral unmixing, and RMS error were computed. Table IV shows the spectral unmixing error for the derived mixed image.

Table IV shows that the spectral unmixing accuracy of each individual land cover type in spectral unmixing is over 80%. Accuracies of water and high moisture vegetation, up to 92.6% and 91.8%, respectively, indicate that the fraction abundance of all endmembers is suitable for subsequent subpixel mapping application.

Based on the seven fraction abundance images (Fig. 14), the subpixel number in each pixel was known for every land cover type. Subpixel mapping images of the derived mixed image were generated using the linear optimization, pixel swapping, spatial attraction model, and our proposed methods. Fig. 15 shows images generated by these four methods.

TABLE IV
ERROR OF SPECTRAL UNMIXING FOR DERIVED MIXED IMAGE

Land cover type	Accuracy
High moisture vegetation	91.8%
Low moisture vegetation	89.5%
Water	92.6%
Shade	81.8%
High albedo impervious surface	82.7%
Low albedo impervious surface	81.9%
Soil	82.4%
Overall accuracy	85.1%
RMS error	0.0807

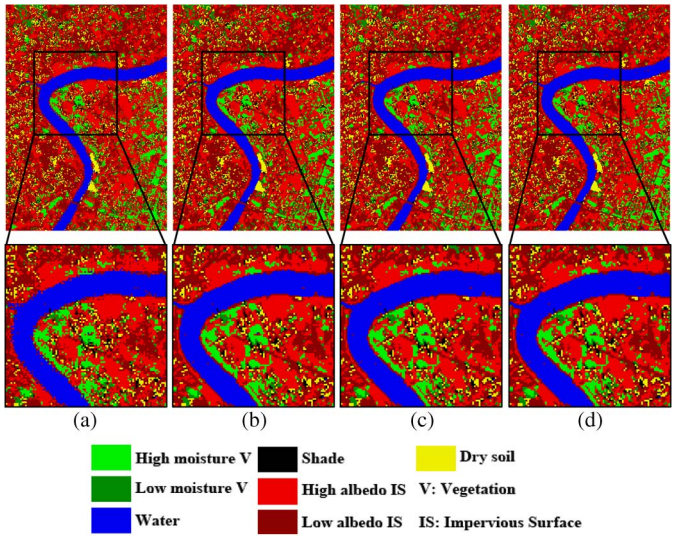

Fig. 15. Mapped images from pyramid mixture model-derived mixed image, using the four methods ($\varsigma = 2$). (a) Linear optimization method, (b) pixel swapping method, (c) spatial attraction model method, and (d) our proposed method.

Spatial resolution of the image in Fig. 15 is 30 m × 30 m, the same as that of the original experimental image. We see in this figure that feature clarity in the images mapped by both the pixel swapping and spatial attraction model methods is much better than that of the linear optimization method and is similar to that of the proposed method at scale factor $\varsigma = 2$.

Based on subpixel mapping with the derived mixed image generated by the pyramid mixture model, overall accuracy and RMS error were obtained for evaluating the four mapping methods, using the spatial sampling units. Each sample pixel in the mapped image ($\varsigma = 2$) was also scaled from the position in the derived mixed image to the same position in the original experimental image. The ground truth land cover type at this position can thus be determined by man-machine interaction. Table V shows the error assessment for the four methods.

From Table V, we see that: 1) Overall accuracy and RMS error of subpixel mapping using the linear optimization method

TABLE V
ERROR ASSESSMENT FOR THE FOUR SUBPIXEL MAPPING METHODS BASED ON THE PYRAMID MIXTURE MODEL($\varsigma = 2$)

	Linear optimization	Pixel swapping	Spatial attraction model	Our proposed method
Overall accuracy	0.5872	0.7213	0.7525	0.8157
RMS error	0.1804	0.0776	0.0613	0.0490

are worse than those using the pixel swapping method for $\varsigma = 2$. 2) The spatial attraction model method yields a better mapping result than the pixel swapping method. 3) The proposed method produces the best result, with overall accuracy 0.8157.

Through comparison of the four methods, we conclude that the linear optimization method is the poorest overall in subpixel mapping. Atkinson's pixel swapping method has greater accuracy. The spatial attraction model method of Mertens *et al.* (2006) [31] shows much improvement over these two. Nevertheless, comparison of visualization quality and quantitative assessment of subpixel mapping images demonstrates that the proposed method performs best in subpixel image mapping, relative to the other three methods. This comparison also indicates that the method based on the pyramid mixture model can effectively measure performance of subpixel mapping, when ground truth samples and contemporaneous high-resolution images are unavailable.

E. Visualization Comparison of Subpixel Mapping Using Hyperion Hyperspectral Image With Larger Size

To illustrate performance of the proposed method on a larger size image, an entire strip of an EO-1 Hyperion hyperspectral image from 2006 [Fig. 1(b)] was used in a comparison. Spectral unmixing was done using the aforementioned 10-EM model. Three scale factors, $\varsigma = 2$, $\varsigma = 5$, and $\varsigma = 8$, were considered. Subpixel images with improved spatial resolution were achieved. These mapped images are shown in Figs. 16–18.

From the results in Figs. 16–18 (enlarged figures), we see that the proposed subpixel mapping method outperforms the other three methods, in terms of overall accuracy. The proposed method can still achieve increased overall accuracy even with a larger image size, particularly at a larger scale factor.

F. Impact of Spectral Mixture Model on Error of Subpixel Mapping

In subpixel mapping, many factors such as the spectral mixture model affect the algorithm and location accuracy. Therefore, in this section, the impact of the spectral mixture model on subpixel mapping accuracy is addressed. Fraction abundance images can be obtained precisely, based on spectral mixture analysis using endmembers combining various land cover types. This analysis, determined by the spectral mixture model defined as n-EM with n endmembers, can affect subpixel mapping accuracy. To investigate this potential effect, a subpixel mapping experiment was conducted by creating different

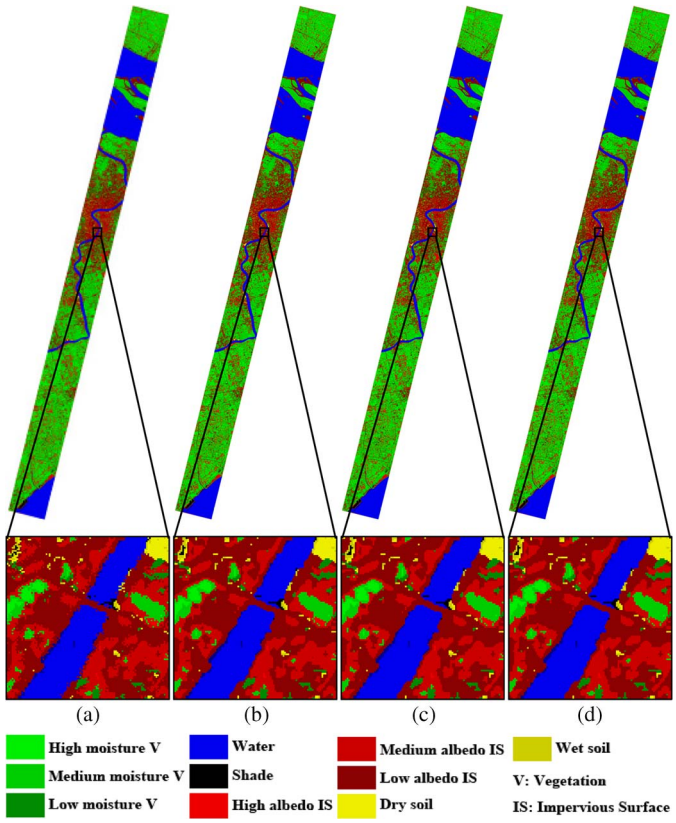

Fig. 16. Mapped images for entire strip of Hyperion hyperspectral image of 2006 ($\varsigma = 2$). (a) Linear optimization method, (b) pixel swapping method, (c) spatial attraction model method, and (d) our proposed method.

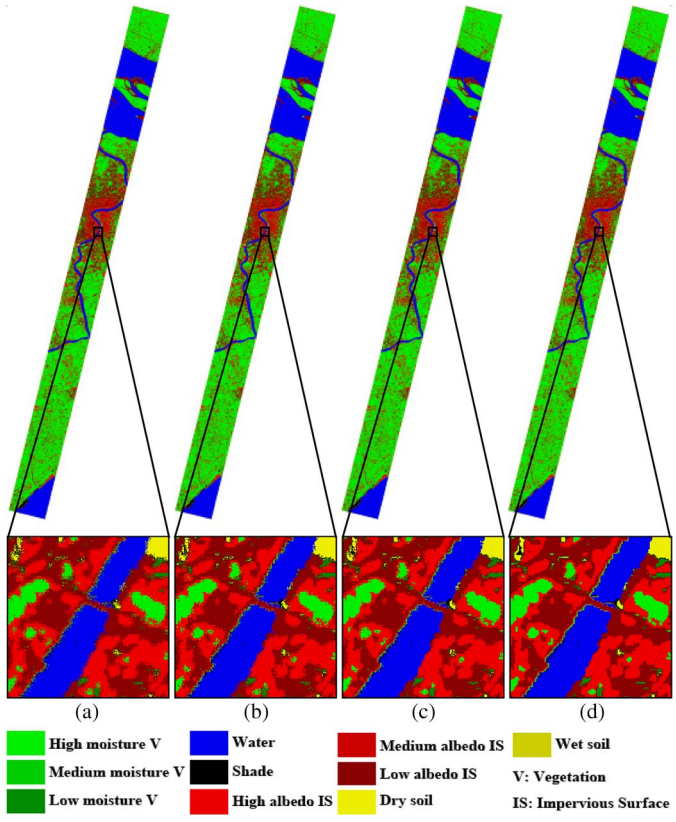

Fig. 17. Mapped images for entire strip of Hyperion hyperspectral image of 2006 ($\varsigma = 5$). (a) Linear optimization method, (b) pixel swapping method, (c) spatial attraction model method, and (d) our proposed method.

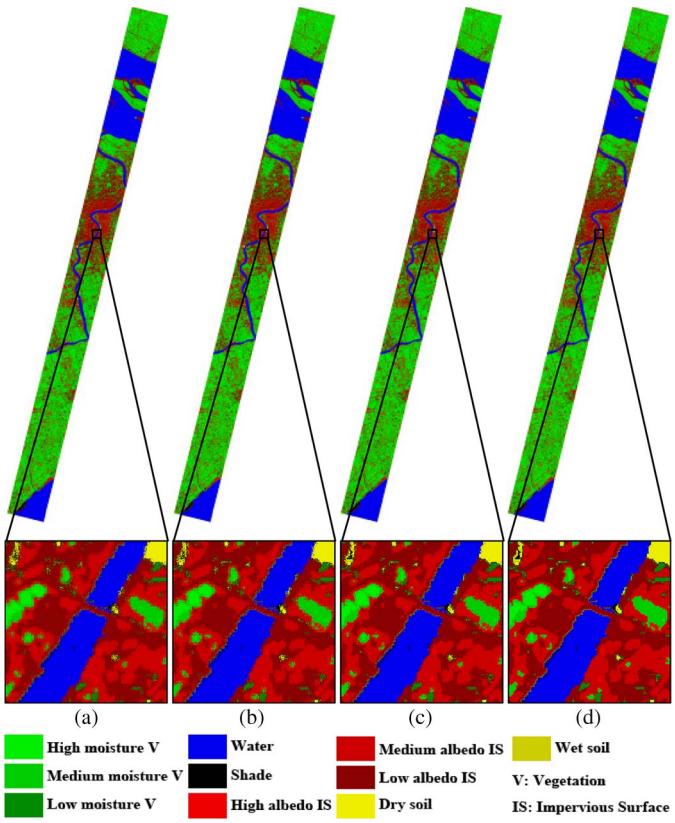

Fig. 18. Mapped images for entire strip of Hyperion hyperspectral image of 2006 ($\varsigma = 8$). (a) Linear optimization method, (b) pixel swapping method, (c) spatial attraction model method, and (d) our proposed method.

spectral mixture models with different endmember sets. These sets were used to do the subpixel mapping, and corresponding subpixel images were generated from the original experimental image using the proposed method at scale factor $\varsigma = 8$. Fig. 19 shows these resultant subpixel images.

From the result in Fig. 19, we see that there are significant differences between the resultant subpixel mapping images. The subpixel image generated using the 3-EM model is the worst at subpixel mapping [see Fig. 19(a)], whereas images generated using the 4-EM to 6-EM models [Fig. 19(b)–(d)] show dramatic improvements in quality. However, image quality from the 6-EM and subsequent models varies little [Fig. 19(d)–(h)]. Fig. 19 shows the relationship between the subpixel mapping accuracy and different n-EM spectral mixture models.

From the results in Figs. 19 and 20, we see that: 1) The various n-EM spectral mixture models can affect the error of subpixel mapping, thereby generating subpixel images with different errors. Generally, the larger the number of endmembers in the spectral mixture model, the higher the overall mapping accuracy and quality of subpixel images. 2) Overall accuracy of subpixel mapping using the 3-EM model is the poorest, at 47.9%. This accuracy using the 10-EM model is the best, with close to 68% at scale factor of $\varsigma = 8$. Overall accuracies increase rapidly from the 3-EM to 6-EM models and smoothly from the 6-EM to 10-EM models. This result shows an inflection point near the exact number of endmembers in the image (e.g., 5-EM). As shown in Fig. 20, before this inflection point,

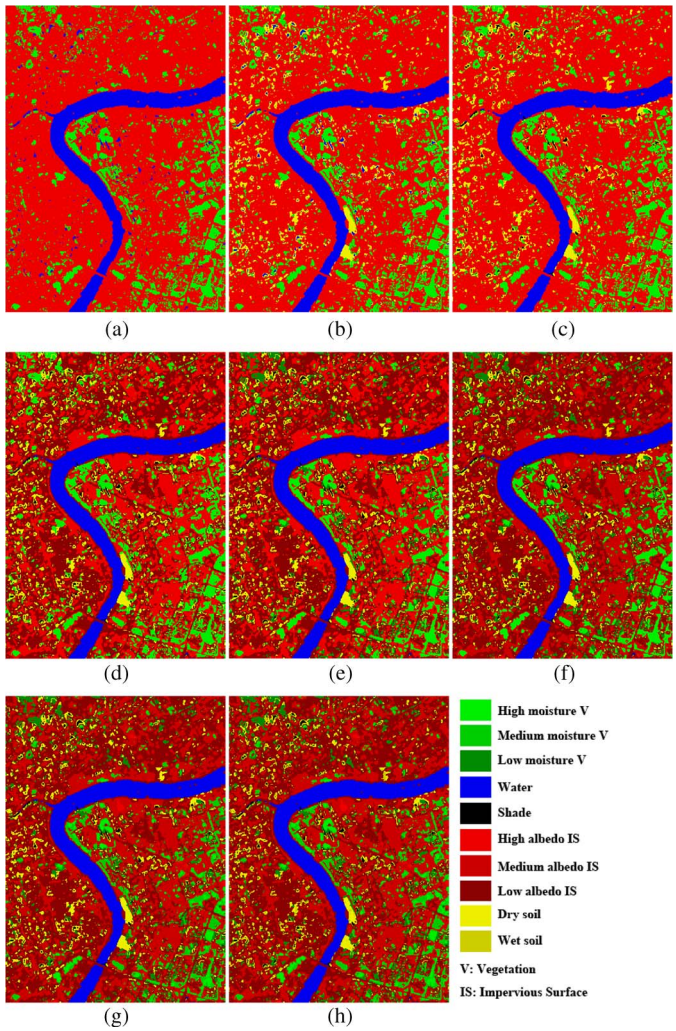

Fig. 19. Subpixel images generated by proposed method, based on different spectral mixture models with different endmember sets ($\varsigma = 8$). (a) Mapped image (3-EM). (b) Mapped image (4-EM). (c) Mapped image (5-EM). (d) Mapped image (6-EM). (e) Mapped image (7-EM). (f) Mapped image (8-EM). (g) Mapped image (9-EM). (h) Mapped image (10-EM).

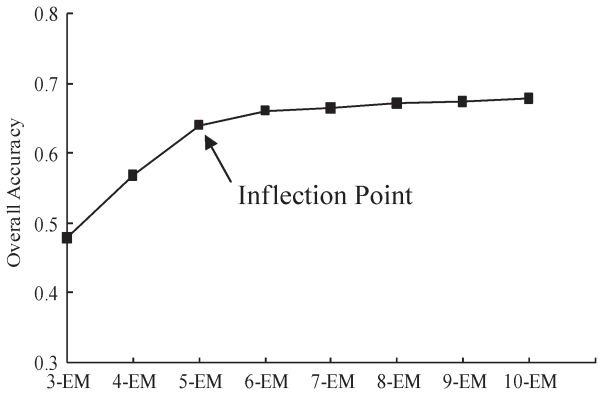

Fig. 20. Relationship between overall accuracy of subpixel mapping and different n-EM spectral mixture models.

overall mapping accuracy increases rapidly; after this point, overall accuracy increases much more smoothly and slowly. The reason for this pattern might be that more endmembers in the spectral mixture model can represent more plentiful and

realistic features of land cover types in the subpixel image, relative to ground truth. On the contrary, fewer endmembers may be unable to represent ground truth well, with scarce features of land cover type in the image.

Therefore, for a linear spectral mixture model with only limited independent endmembers (e.g., one to three endmembers) in the image, many pixels associated with complicated ground objects may not be well represented by such few endmember spectra. This results in a low accuracy in generating the subpixel mapping image. For a linear spectral mixture model with increased endmembers (e.g., five), most pixels in the image can be represented linearly by the endmembers, and the spectral unmixing result would be more accurate. This would improve the accuracy of subpixel mapping. However, when there are more than five endmembers in a linear spectral mixture model, image accuracy increases slowly with endmember number in that model.

V. Conclusion

To address the disadvantages of traditional subpixel mapping methods that simply describe spatial dependence relying on attractive correlation, this paper presents a new subpixel mapping method, based on attraction-repulsion between subpixels. The proposed method yields more accurate subpixel mapping, based on spectral mixture analysis. Through a comprehensive comparison (based on a schematic diagram, visualization assessment, and quantitative analysis) of the proposed method and three traditional methods, the following conclusions are reached.

1) The proposed subpixel mapping method can better retrieve the spatial dependence of ground truth, using attraction-repulsion correlation between subpixels. The proposed method makes use of spatial dependence with attraction between the same kinds of ground objects, plus repulsion between different kinds of these objects. With the introduction of repulsion, the proposed method performs better in grouping subpixels of the same land cover type together, rather than isolating subpixels from the sets of the same land cover type. Moreover, the proposed method is capable of processing multiple fractions of land cover types for representing ground truth in more detail, based on the attraction and repulsion. Therefore, this method achieves better performance in subpixel mapping than the other three methods (linear optimization, pixel swapping, and spatial attraction model). The method can generate a subpixel image with better visualization quality than the other three, and it performs more accurate subpixel mapping in subpixel locations.
2) Relative to the other methods, the proposed method can obtain better outcomes with more robust accuracy at all scale factors, particularly larger ones. As the scale factor increases, subpixel mapping accuracy decreases with all four mapping methods.
3) The pyramid mixture model is an effective way to evaluate performance of subpixel mapping, particularly in the case where ground truth samples or contemporaneous high-resolution reference images are unavailable.
4) Analysis of the impact of different n-EM spectral mixture models on subpixel mapping accuracy shows that the larger the number of endmembers in the spectral mixture model, the higher the overall accuracy of subpixel mapping and quality of the subpixel image. In addition, there is an inflection point near the exact number of endmembers in the image (e.g., 6-EM); after this point, subpixel mapping accuracy increases smoothly but slowly.

With improved spatial resolution of subpixel mapping based on the proposed method, the derived images can be used for precise classification of land cover types. Subpixel mapping has been extended from its current use on raster imagery to a vector data application, for refining location estimates of ground control points [55]. The enhancement of image spatial resolution from subpixel mapping cannot match improvement from hardware-based techniques. However, given certain hardware, the subpixel mapping approach could be used in many fields that require higher spatial resolution imagery. Finally, there are some limitations of the proposed algorithms. For example, the approach is based on spatial dependence between subpixels; thus, it might be suitable only for mapping ground objects larger than the size of a pixel. As a result, many small objects within a pixel might be estimated incorrectly. Therefore, future research will focus on a method that can locate objects smaller than a pixel.

Acknowledgment

The authors greatly appreciate the valuable comments and suggestions of the anonymous reviewers. Part of the work was completed when Dr. X. Zhang was a visiting student at Purdue University under the support of China Scholarship Council Scholarship between 2009 and 2010.

References

[1] G. M. Foody, *Remote Sensing Image Analysis: Including the Spatial Domain*. Norwell, MA: Kluwer, 2004, pp. 37–49.
[2] A. P. Cracknell, "Synergy in remote sensing—What's in a pixel?" *Int. J. Remote Sens.*, vol. 19, no. 11, pp. 2025–2047, 1998.
[3] P. Fisher, "The pixel: A snare and a delusion," *Int. J. Remote Sens.*, vol. 18, no. 3, pp. 679–685, 1997.
[4] J. Fryer and K. McIntosh, "Enhancement of image resolution in digital photogrammetry," *Photogramm. Eng. Remote Sens.*, vol. 67, no. 6, pp. 741–749, Jun. 2001.
[5] J. M. P. Nascimento and J. M. B. Dias, "Does independent component analysis play a role in unmixing hyperspectral data?" *IEEE Trans. Geosci. Remote Sens.*, vol. 43, no. 1, pp. 175–187, Jan. 2005.
[6] C. A. Shah, P. K. Varshney, and M. K. Arora, "ICA mixture model algorithm for unsupervised classification of remote sensing imagery," *Int. J. Remote Sens.*, vol. 28, no. 8, pp. 1711–1731, Apr. 2007.
[7] F. A. Kruse, A. B. Lefkoff, J. W. Boardman, K. B. Heidebrecht, A. T. Shapiro, and P. J. Barloon, "The spectral image-processing system (SIPS)—Interactive visualization and analysis of imaging spectrometer data," *Remote Sens. Environ.*, vol. 44, no. 2/3, pp. 145–163, May/Jun. 1993.
[8] N. Goodwin, N. C. Coops, and C. Stone, "Assessing plantation canopy condition from airborne imagery using spectral mixture analysis and fractional abundances," *Int. J. Appl. Earth Observ. Geoinf.*, vol. 7, no. 1, pp. 11–28, May 2005.
[9] S. W. Myint, "Urban vegetation mapping using sub-pixel analysis and expert system rules: A critical approach," *Int. J. Remote Sens.*, vol. 27, no. 13, pp. 2645–2665, 2006.
[10] J. Tang, L. Wang, and S. W. Myint, "Improving urban classification through fuzzy supervised classification and spectral mixture analysis," *Int. J. Remote Sens.*, vol. 28, no. 18, pp. 4047–4063, Sep. 2007.

[11] A. M. De Asis and K. Omasa, "Estimation of vegetation parameter for modeling soil erosion using linear spectral mixture analysis of Landsat ETM data," *ISPRS J. Photogramm. Remote Sens.*, vol. 62, pp. 309–324, 2007.

[12] L. C. Plourde, S. V. Ollinger, M. L. Smith, and M. E. Martin, "Estimating species abundance in a northern temperate forest using spectral mixture analysis," *Photogramm. Eng. Remote Sens.*, vol. 73, no. 7, pp. 829–840, Jul. 2007.

[13] T. C. Eckmann, D. A. Roberts, and C. J. Still, "Using multiple endmember spectral mixture analysis to retrieve sub-pixel fire properties from MODIS," *Remote Sens. Environ.*, vol. 112, no. 10, pp. 3773–3783, Oct. 2008.

[14] N. Richter, K. Staenz, and H. Kaufmann, "Spectral unmixing of airborne hyperspectral data for baseline mapping of mine tailings areas," *Int. J. Remote Sens.*, vol. 29, no. 13, pp. 3937–3956, Jul. 2008.

[15] Q. Weng, X. Hu, and D. Liu, "Extracting impervious surfaces from medium spatial resolution multispectral and hyperspectral imagery: A comparison," *Int. J. Remote Sens.*, vol. 29, no. 11, pp. 3209–3232, Jun. 2008.

[16] Q. Weng, X. Hu, and H. Liu, "Estimating impervious surfaces using linear spectral mixture analysis with multitemporal ASTER images," *Int. J. Remote Sens.*, vol. 30, no. 18, pp. 4807–4830, Sep. 2009.

[17] B. Somers, S. Delalieux, J. Stuckens, W. W. Verstraeten, and P. Coppin, "A weighted linear spectral mixture analysis approach to address endmember variability in agricultural production systems," *Int. J. Remote Sens.*, vol. 30, no. 1, pp. 139–147, Jan. 2009.

[18] T. R. Tooke, N. C. Coops, N. R. Goodwin, and J. A. Voogt, "Extracting urban vegetation characteristics using spectral mixture analysis and decision tree classifications," *Remote Sens. Environ.*, vol. 113, no. 2, pp. 398–407, Feb. 2009.

[19] L. Zhang, B. Wu, B. Huang, and P. Li, "Nonlinear estimation of subpixel proportion via kernel least square regression," *Int. J. Remote Sens.*, vol. 28, no. 18, pp. 4157–4172, Sep. 2007.

[20] B. Somers, K. Cools, S. Delalieux, J. Stuckens, D. V. der Zande, W. W. Verstraeten, and P. Coppin, "Nonlinear hyperspectral mixture analysis for tree cover estimates in orchards," *Remote Sens. Environ.*, vol. 113, no. 6, pp. 1183–1193, Jun. 2009.

[21] J. Ju, E. D. Kolaczyk, and S. Gopal, "Gaussian mixture discriminant analysis and sub-pixel land cover characterization in remote sensing," *Remote Sens. Environ.*, vol. 84, no. 4, pp. 550–560, Apr. 2003.

[22] D. Lafont and B. Guillemet, "Beam-filling effect correction with subpixel cloud fraction using a neural network," *IEEE Trans. Geosci. Remote Sens.*, vol. 43, no. 5, pp. 1070–1077, May 2005.

[23] J. Ravi, S. T. Lee, M. Paulraj, and R. Hernandez, "Feasibility of neural network approach in spectral mixture analysis of reflectance spectra," *Int. J. Remote Sens.*, vol. 29, no. 10, pp. 2981–2992, May 2008.

[24] R. Pu, P. Gong, R. Michishita, and T. Sasagawa, "Spectral mixture analysis for mapping abundance of urban surface components from the Terra/ASTER data," *Remote Sens. Environ.*, vol. 112, no. 3, pp. 939–954, Mar. 2008.

[25] J. Verhoeye and R. de Wulf, "Land cover mapping at sub-pixel scales using linear optimization techniques," *Remote Sens. Environ.*, vol. 79, no. 1, pp. 96–104, Jan. 2002.

[26] D. Lu and Q. Weng, "A survey of image classification methods and techniques for improving classification performance," *Int. J. Remote Sens.*, vol. 28, no. 5, pp. 823–870, Feb. 2007.

[27] X. H. Tong, X. Zhang, and M. L. Liu, "Detection of urban sprawl using a genetic algorithm-evolved artificial neural network classification in remote sensing: A case study in Jiading and Putuo districts of Shanghai, China," *Int. J. Remote Sens.*, vol. 31, no. 6, pp. 1485–1504, Feb. 2010.

[28] P. M. Atkinson, *Mapping Sub-pixel Boundaries From Remotely Sensed Images. Innovations in GIS 4*, Z. Kemp, Ed. Bristol, PA: Taylor & Francis, 1997, pp. 166–180.

[29] P. M. Atkinson, "Super-resolution target mapping from soft classified remotely sensed imagery," *Photogramm. Eng. Remote Sens.*, vol. 71, no. 7, pp. 839–846, Jul. 2005.

[30] K. C. Mertens, L. P. C. Verbeke, T. Westra, and R. R. De Wulf, "Subpixel mapping and sub-pixel sharpening using neural network predicted wavelet coefficients," *Remote Sens. Environ.*, vol. 91, no. 2, pp. 225–236, May 2004.

[31] K. C. Mertens, B. De Baets, L. P. C. Verbeke, and R. R. De Wulf, "A sub-pixel mapping algorithm based on sub-pixel/pixel spatial attraction," *Int. J. Remote Sens.*, vol. 27, no. 15, pp. 3293–3310, Jan. 2006.

[32] Y. Makido, A. Shortridge, and J. P. Messina, "Assessing alternatives for modeling the spatial distribution of multiple land-cover classes at sub-pixel scales," *Photogramm. Eng. Remote Sens.*, vol. 73, no. 8, pp. 935–943, Aug. 2007.

[33] Y. Makido and A. Shortridge, "Weighting function alternatives for a subpixel allocation model," *Photogramm. Eng. Remote Sens.*, vol. 73, no. 11, pp. 1233–1240, Nov. 2007.

[34] Z. Shen, J. Qi, and K. Wang, "Modification of pixel swapping algorithm with initialization from a sub-pixel/pixel spatial attraction model," *Photogramm. Eng. Remote Sens.*, vol. 75, no. 5, pp. 557–567, May 2009.

[35] G. M. Foody, "Sharpening fuzzy classification output to refine the representation of sub-pixel land cover distribution," *Int. J. Remote Sens.*, vol. 19, no. 13, pp. 2593–2599, 1998.

[36] M. W. Thornton, P. M. Atkinson, and D. A. Holland, "Sub-pixel mapping of rural land cover objects from fine spatial resolution satellite sensor imagery using super-resolution pixel swapping," *Int. J. Remote Sens.*, vol. 27, no. 3, pp. 473–491, 2006.

[37] T. Kasetkasem, M. K. Arora, and P. K. Varshney, "Super-resolution land cover mapping using a Markov random field based approach," *Remote Sens. Environ.*, vol. 96, no. 3/4, pp. 302–314, Jun. 2005.

[38] A. Boucher and P. C. Kyriakidis, "Super-resolution land-cover mapping with indicator geostatistic," *Remote Sens. Environ.*, vol. 104, no. 3, pp. 264–282, Oct. 2006.

[39] A. Boucher and P. C. Kyriakidis, "Integrating fine scale information in superresolution land cover mapping," *Photogramm. Eng. Remote Sens.*, vol. 73, no. 8, pp. 913–921, Aug. 2007.

[40] M. Debella-Gilo and A. Kääb, "Sub-pixel precision image matching for measuring surface displacements on mass movements using normalized cross-correlation," *Remote Sens. Environ.*, vol. 115, no. 1, pp. 130–142, Jan. 2011.

[41] H. N. Gross and J. P. Schott, "Application of spatial resolution enhancement and spectral mixture analysis to hyperspectral image," in *Proc. SPIE*, 1996, vol. 2821, pp. 30–41.

[42] H. N. Gross and J. P. Schott, "Application of spectral mixture analysis and image fusion techniques for image sharpening," *Remote Sens. Environ.*, vol. 63, no. 2, pp. 85–94, Feb. 1998.

[43] A. J. Tatem, H. G. Lewis, P. M. Atkinson, and M. S. Nixon, "Super-resolution target identification from remotely sensed images using a Hopfield neural network," *IEEE Trans. Geosci. Remote Sens.*, vol. 39, no. 4, pp. 781–796, Apr. 2001.

[44] A. J. Tatem, H. G. Lewis, P. M. Atkinson, and M. S. Nixon, "Multiple-class land-cover mapping at the sub-pixel scale using a Hopfield neural network," *Int. J. Appl. Earth Observ. Geoinf.*, vol. 3, no. 2, pp. 184–190, 2001.

[45] A. J. Tatem, H. G. Lewis, P. M. Atkinson, and M. S. Nixon, "Superresolution land cover pattern prediction using a Hopfield neural network," *Remote Sens. Environ.*, vol. 79, no. 1, pp. 1–14, 2002.

[46] A. J. Tatem, H. G. Lewis, P. M. Atkinson, and M. S. Nixon, "Increasing the spatial resolution of agricultural land cover maps using a Hopfield neural network," *Int. J. Geograph. Inf. Sci.*, vol. 17, no. 7, pp. 647–672, 2003.

[47] M. Q. Nguyen, P. M. Atkinson, and H. G. Lewis, "Super-resolution mapping using a Hopfield neural network with fused images," *IEEE Trans. Geosci. Remote Sens.*, vol. 44, no. 3, pp. 736–749, Mar. 2006.

[48] K. C. Mertens, L. P. C. Verbeke, and E. I. Ducheyne, "Using genetic algorithms in sub-pixel mapping," *Int. J. Remote Sens.*, vol. 24, no. 21, pp. 4241–4247, Nov. 2003.

[49] C. P. Ruiz and F. J. A. Lopez, "Restoring SPOT images using PSF-derived deconvolution filters," *Int. J. Remote Sens.*, vol. 23, no. 12, pp. 2379–2391, 2002.

[50] C. Huang, J. R. G. Townshend, S. Liang, S. N. V. Kalluria, and R. S. DeFries, "Impact of sensor's point spread function on land cover characterization: Assessment and deconvolution," *Remote Sens. Environ.*, vol. 80, no. 2, pp. 203–212, May 2002.

[51] G. Kaiser and W. Schneider, "Estimation of sensor point spread function by spatial sub-pixel analysis," *Int. J. Remote Sens.*, vol. 29, no. 7, pp. 2137–2155, Apr. 2008.

[52] B. Datt, T. R. McVicar, T. G. Van Niel, D. L. B. Jupp, and J. S. Pearlman, "Preprocessing EO-1 hyperion hyperspectral data to support the application of agricultural indexes," *IEEE Trans. Geosci. Remote Sens.*, vol. 41, no. 6, pp. 1246–1259, Jun. 2003.

[53] X. H. Tong, X. Zhang, J. Shan, H. Xie, and M. L. Liu, "Image segmentation based spectral mixture analysis for hyperspectral remotely sensed imagery," *Remote Sens. Environ.*, submitted for publication.

[54] R. G. Congalton, "A review of assessing the accuracy of classifications of remotely sensed data," *Remote Sens. Environ.*, vol. 37, no. 1, pp. 35–46, Jul. 1991.

[55] G. M. Foody, "The role of soft classification techniques in the refinement of estimates of ground control point location," *Photogramm. Eng. Remote Sens.*, vol. 68, no. 9, pp. 897–903, Sep. 2002.

Xiaohua Tong received the Ph.D. degree from Tongji University, Shanghai, China, in 1999.

He worked as a Postdoctoral Researcher in the State Key Laboratory of Information Engineering in Surveying, Mapping, and Remote Sensing, Wuhan University, Wuhan, China, between 2001 and 2003; he was a Research Fellow in The Hong Kong Polytechnic University, Kowloon, Hong Kong, in 2006, and a Visiting Scholar in the University of California, Santa Barbara, between 2008 and 2009. His current research interests include remote sensing, geographic information systems, uncertainty and spatial data quality, image processing for high-resolution and hyperspectral images.

Dr. Tong serves as the Vice Chair of the commission on spatial data quality of International Cartographical Association and a Council Member of Chinese Association of Geographical Information Systems.

Xue Zhang received the B.S. degree in geographical information system from Hunan Normal University, Hunan, China, in 2004, and the M.S. and Ph.D. degrees in cartography and geographical information engineering from Tongji University, Shanghai, China, in 2007 and 2011, respectively.

From 2009 to 2010, he was a Visiting Student in Purdue University, West Lafayette, IN, under the support of the China Scholarship Council Scholarship. His research mainly focuses on multispectral/hyperspectral remote sensing and land cover/use remote sensing. His research interests include pattern recognition of remote sensing image, spectral remote sensing, and its applications.

Jie Shan (M'08) received the Ph.D. degree in photogrammetry and remote sensing from Wuhan University, Wuhan, China, in 1989.

He has held faculty positions with universities in China and Sweden and has been a Research Fellow in Germany. Currently, he is a Professor in geomatics engineering with the School of Civil Engineering, Purdue University, West Lafayette, IN. His area of interests includes sensor geometry, pattern recognition from images and lidar data, object extraction and reconstruction, urban remote sensing, and automated mapping.

Dr. Shan is a recipient of multiple academic awards, among which are the Talbert Abrams Grand Award, the Environmental Systems Research Institute Award for Best Scientific Paper in Geographic Information System (GIS) (First Place), and the Excellence in GIS Award. He has been the Cochair of the Remote Sensing Data Fusion Working Group and the Pattern Recognition for Remote Sensing Working Group, both in the International Society for Photogrammetry and Remote Sensing. He is an Associate Editor for the IEEE TRANSACTIONS GEOSCIENCE AND REMOTE SENSING and the Assistant Editor for *Photogrammetric Engineering and Remote Sensing*. He is also a member of the American Society for Photogrammetry and Remote Sensing, and the American Geophysical Union.

Huan Xie received the B.S. degree in surveying engineering and the M.S. and Ph.D. degrees in cartography and geoinfomation from Tongji University, Shanghai, China, in 2003, 2006, and 2009, respectively.

From 2007 to 2008, she was a Visiting Student in the Institute of Photogrammetry and GeoInformation, Leibniz Universität Hannover, Hannover, Germany, under the support of the China Scholarship Council Scholarship. Since June 2009, she has been working in the College of Surveying and Geo-Informatics, Tongji University. Currently, she is a Lecturer and teaches courses related to remote sensing and geographic information systems. Her research interests include hyperspectral remote sensing and polar remote sensing.

Miaolong Liu received the B.S. degree in geodesy from Wuhan University, Wuhan, China, China, in 1967.

He has held faculty positions with universities and research institutes in China, From 1988 to 1995, he was a Senior Visiting Scholar in the Geography Department in Sheffield University, Sheffield, U.K. Since 1997, he has been a Professor in cartography and geographical information science with the College of Surveying and Geo-Informatics, Tongji University, Shanghai, China. His area of interests includes geographical information sciences, spatial analysis and geocomputation, and land use/cover remote sensing.